THE ASTROPHYSICAL JOURNAL, 350:561–577, 1990 February 20

HOLLOW CONICAL JET MODELS FOR SS 433: A PARADIGM LOST?

CHRISTOPHER S. KOCHANEK
Theoretical Astrophysics, California Institute of Technology

AND

JOHN F. HAWLEY
Department of Astronomy, University of Virginia
Received 1988 October 13; accepted 1989 August 18

ABSTRACT

A precessing jet can be approximated as an axisymmetric flow if the precession time is short compared to the propagation time over scales of interest. An example is the jet in SS 433, where the precession time is $\simeq$0.5 yr and the propagation time from SS 433 to the W50 remnant is $\gtrsim$1000 yr. We perform a series of simulations of precessing jets using a $R - Z$ (axisymmetric) finite difference hydrodynamics code. We reproduce first the results for the *filled jets* studied previously by several groups. Next, we examine *hollow cylindrical jets*, which allow us to examine the effects of a hollow jet without the complications of a growing interior volume. This case may serve as a "postfocusing" model of a precessing jet. Finally, we examine *hollow conical jets*, which model the behavior of a precessing jet propagating on the surface of its precession cone. The conical jets "stall" at the point where the momentum flux density in the jet becomes too low to push the ambient gas from its path. If the area of the working surface over which the jet transfers momentum to the ambient medium is A_w, the area of the jet orifice is A_j, and the initial internal Mach number of the jet is M_j, the jet stalls when $A_w = M_j^2 A_j$. The jet propagates in an extremely unsteady fashion, with large radial oscillations in the position of the jet's channel. The oscillations cause A_w to grow proportional to R^2, where R is the outer radius of the jet, so that the jet stalls at $R \simeq M_j R_0$, where R_0 is the initial outer radius of the jet. The oscillations of the jet are caused by the competition between the supersonic vortices, which make up the cocoon about the exterior of the jet, and the shocked ambient gas on the interior of the jet. While the cocoon can induce a temporary focusing of the jet, the pressure in the interior is able to prevent any permanent focusing. The bow shocks of the hollow jets are much flatter than those of the filled jets, and no feature which resembles the "ears" of the W50 remnant develops. It seems unlikely that the "ears" of W50 can be formed by a *hydrodynamic jet* ejected with a precession cone as large as that currently observed in the SS 433 system.

Subject headings: galaxies: jets — hydrodynamics — nebulae: individual (W50) — stars: individual (SS 433)

I. INTRODUCTION AND MOTIVATION

High-energy radio jets have inspired an extensive series of numerical hydrodynamics simulations. Although these calculations have not in the strictest sense served as *models* for any extragalactic radio jet, they have proved valuable in exploring and understanding the physics of supersonic jets. Most of these simulations have been two-dimensional, axisymmetric, or slab symmetric models, both with and without magnetic fields. Exotic jet geometries have yet to be examined in detail, because they are less relevant than the collimated cylinder. There are, however, a few restricted cases in which more exotic flow geometries are required. In particular, the galactic source SS 433 is modeled naturally by injecting the jet into the ambient medium on the surface of a cone: a hollow, conical jet instead of a filled, cylindrical, canonical jet.

The object SS 433 is a unique example of a radio jet, one for which we have extensive observations and excellent kinematic information (reviewed by Margon 1984). The time-varying Doppler shifts observed in the emission lines of the system are believed to originate in two opposing jets with velocities of 0.26*c*, processing with a period of 164 days on the surface of a cone with a half-angle of 20°. VLA observations on scales of 0".1–0".5 (Hjellming and Johnston 1982, 1985) confirm this picture, revealing regions of emission arranged in a helical pattern, which are interpreted as the instantaneous pattern of ejected knots of emission on the precession cone. VLBI observations on scales of 50–300 mas (Vermeulen *et al.* 1987) are also consistent with a series of emitting clumps of gas moving along the helical trajectory predicted by the kinematic model. These direct observations of the precessing jet, along with the kinematic model for the system, place SS 433 at a distance of 5.5 kpc (1" = 0.03 pc at 5.5 kpc).

Surrounding SS 433 is the asymmetric radio shell (and possible supernova remnant) W50, which has a width along the center of the jet precession cone (the major axis) of about 2° (Downes, Pauls, and Salter 1986). The width along the minor axis is about 1° (= 97 pc at D = 5.5 kpc). W50 is notable for its asymmetry, in particular the presence of "ears," or projections that coincide with the precession cone axes of the radio jets. The coincidence of alignment between the jet axis and the ears leads to the paradigm for the jet in SS 433: the ears of W50 are formed by the dynamical effects of the jet. If the precession cone is drawn about the axis, the bulges have a half angle of 10°–15° compared with the 20° half-angle of the jet as seen on the VLA scale. Hence, the paradigm also assumes that the jet is partially focused relative to its precession cone as it propagates.

There is some evidence other than the alignment of the jets and the ears to support the picture of interaction between the jets and W50. Optical filaments have been detected near the inner edge of the ears and within the precession cone (Zealey, Dopita, and Malin 1980; Kirshner and Chevalier 1980). X-ray observations of the system (Watson *et al.* 1983) reveal bright diffuse lobes of emission lying along the major axis of W50 at distances ranging from 25 to 70 pc. The peak of the emission is well within the precession cone of the jets, although some emission is detected outside of the limits defined by the cone. The assumption is that the jets are responsible for both the optical emission and for energizing and confining these X-ray lobes.

The specific model for the system is the hydrodynamical *hollow*, conical jet (Begelman *et al.* 1980; Davidson and McCray 1980; Königl 1983). The jet drives shocks into the interior of the precession cone, heating the ambient or jet cocoon gas to X-ray luminescence. The jet terminates at the edge of W50, producing the ears. Some focusing or collimation is required to account for the reduced angular size of the ears. While this overall picture is appealing, it is not based upon a rigorous examination of the physics of such a jet. Several key questions remain unanswered. What is the jet geometry out in the region of 30–100 pc from SS 433? How do what appear to be ballistic knots of high-energy plasma seen at small radii by the VLA become hydrodynamic? How does a hydrodynamic hollow jet produce and confine the X-ray lobes and energize the ears? Do precessing jets collimate or focus themselves as they propagate through an ambient medium?

These questions can be answered in detail only through numerical simulations of the propagation of hollow conical jets. While our simulations are certainly inspired by the SS 433 system, they do not represent an attempt to make a detailed model of the system; at this point, we can only hope to gain a qualitative understanding of the physical behavior of a hollow jet. To establish the context for our simulations, we begin with a discussion of some of the details that frame the key issues. First, under what conditions can the jet in SS 433 be modeled as an axisymmetric, hydrodynamic jet? The optical line profiles and the radio data present a picture of material ejected coherently on time scales of a few hours. If we assume the jet does not slow down appreciably in the distance to the remnant, the time required for it to flow from SS 433 to W50 is approximately 1000 yr ($t_p \simeq 1000$ yr); in this time the jet will have precessed 2000 times. If the jet slows on larger scales (where there is no observational data on the velocity of the jet), the propagation time could be considerably extended, increasing the winding number. At the maximum speed of 0.26c, the separation between loops of the precessing jet is less than 0.04 pc. The "bullets" or "blobs" of gas will expand either because they are overpressured with respect to the ambient medium or because of the internal velocity dispersion in the gas. The expansion due to internal pressure will occur at the sound speed of the gas, which for gas at a temperature of 10^4 K is $c_s \sim 10$ km s^{-1}. While there is evidence on the radio scales that the bullets are expanding adiabatically (Vermeulem *et al.* 1987; Hjellming and Johnston 1988), such expansion alone will not fill in the interbullet spacing. The sound speed is so much smaller than the propagation velocity ($c_s/v_j \sim 10^{-4}$) that the expansion of the material is much more likely to be dominated by the velocity dispersion of the jet, δv. If the jet has a velocity dispersion δv, then the time scale to fill in the gaps between successive coils of the jet is $t_f \simeq t_{\rm precess}\, v_j/\delta v$, which for a 1% velocity dispersion ($\delta v/v_j = 0.01$) is $t_f \simeq 50$ yr—a small fraction of the time to reach the remnant (compared to $t_f = t_{\rm precess}\, v_j/c_s \simeq 5000$ yr for adiabatic expansion). The current upper limit on the velocity dispersion is $\delta v/v_j < 0.04$ (Milgrom, Anderson, and Margon 1982). Hence, unless the bullets are generated with a remarkably low velocity dispersion, a precessing jet such as SS 433 can be modeled as being axisymmetric about the precession axis on scales that are large compared to the region in which the jet is generated.

Next, can we expect a hollow, conical jet to focus? Eichler (1983) proposed a simple analytic model for focusing hollow jets through interactions with the ambient medium and an *assumed* zero pressure region inside the cone. In the absence of a gravitational potential, or other external momentum sink, the ambient medium cannot provide a time-independent mechanism for focusing. Momentum transfer to the ambient medium must eventually drive it out of the path of the jet. An external medium can only induce a *temporary* focusing effect. In Eichler's (1983) model, it is the assumed zero pressure region that leads to focusing. Whether or not this is a viable mechanism depends upon the hydrodynamics and the existence of a mechanism for cooling the interior gas on the dynamical time scale. In our present study, we ignore cooling and concentrate upon the gas dynamics of a traditional ideal-gas jet. If such a jet is to be focused solely by a hydrodynamic mechanism for many dynamical times, it must occur through "self-interactions" between the jet and its cocoon. We know from numerical studies of filled jets that their dynamics are dominated by their cocoons (Norman *et al.* 1982, hereafter NSW82; Norman, Winkler, and Smarr 1983, 1984, hereafter NWS83,84; Norman and Winkler 1985, hereafter NW85; Kössl and Müller 1988, hereafter KM88; Lind *et al.* 1988, hereafter LPMB88), and we have the same expectation for the hollow jets.

Through simulation, we can test many of the hypotheses that underly the current paradigm for the jet in SS 433. Our primary assumptions are that the jet is hydrodynamic and approximately axisymmetric on large scales. In § II, we describe the numerical method and the initial data used in the simulations, and we compare some cylindrical test jets with previous calculations in the literature. In § III, we discuss some general analytic considerations governing the propagation of jets. In § IV, we describe the results of our numerical experiments comparing three different jet geometries: filled jets, *hollow cylindrical jets*, and *hollow conical jets*. The jet Mach numbers and density ratios are chosen to cover the two major regimes of stable, highly supersonic jet propagation: the light, cocoon-dominated jets, and the heavy, ballistic or "naked beam" jets. Finally, in § V, we discuss the consequences of these simulations for the jet paradigm in the SS 433 system.

II. THE NUMERICAL METHOD

We wish to consider the dynamical properties of a hydrodynamic jet propagating along the surface of a hollow, axisymmetric cone. We study three basic jet configurations: the *hollow cone*, in which the jet is injected with a fixed annular width on a cone with a $\theta_c = 20°$ half-angle opening, the *hollow cylinder*, a jet with fixed annular width injected parallel to the axis, and the now standard cylindrical *filled jet*. Although there is interest in considering the effects of nonuniform and nonstationary ambient media on jet propagation, we choose to keep our initial study as simple as possible, given that we are working with a novel jet geometry. Therefore, the ambient medium is stationary, homogeneous, and isentropic.

For this study, we developed a time-explicit, Eulerian finite-difference, Newtonian hydrodynamics code in cylindrical $R-Z$ coordinates. The numerical techniques employed are the same as those described in Hawley, Smarr, and Wilson (1984), viz. van Leer's monotonic transport scheme. We calibrated the code using both one-dimensional (e.g., standard shock tube, Sedov line explosion) and two-dimensional (e.g., spherical Sedov explosion in cylindrical coordinates) test problems. We have also made direct comparisons to the published results of NWS83, NWS84, KM88, and LPMB88. These comparisons are particularly useful because, in addition to testing our code, they provide insights into the reasons behind the quantitative differences in the jets obtained by different groups. All codes in our comparison sample are two-dimensional and time explicit. NWS83, NWS84, and LPMB88 use the same monotonic transport scheme used in our code, while KM88 use the flux-corrected transport scheme. LPMB88 also employ a total rather than an internal energy equation in the hydrodynamics.

For the simulations, we use units in which the ambient pressure P_a and density ρ_a are set equal to 1. The length scale is the radius of the filled jet $R_j \equiv 1$. This gives a time scale $t_i = R_j(P_a/\rho_a)^{-1/2}$, which is the *isothermal* sound crossing time across the jet. LPMB88 use the same units, while NWS83, NWS84, and KM88 use the sound crossing time $t_s = \Gamma^{-1/2} t_i$. The input parameters are the jet density $\rho_j \equiv \eta \rho_a$ and the jet internal Mach number $M_j = v_j/c_j$. The jet is injected in pressure equilibrium with the ambient medium $P_j = P_a$. The hollow cylindrical jets have an inner radius of $3/4R_j$, and an outer radius of $5/4R_j$, corresponding to a thickness to mean radius ratio of $\Delta R/\bar{R} = \frac{1}{2}$. The hollow conical jets use the same inner and outer radii as the hollow cylindrical jets, but the velocities lie on a cone with a half-angle of 20°. The filled jet and the hollow cylindrical jet have, by design, the same mass, energy, and momentum fluxes. The fluxes in the conical case are a factor of 1/cos 20° = 1.06 times larger, because the grid zone size and spacing limit the adjustments possible to compensate for the angle the velocity vector makes with respect to the grid. In all cases, $\Gamma = 5/3$ ideal gas equation of state is used.

The simulations are performed on a 256 × 512 $R - Z$ grid. In the axial direction, the zone width is 1/20 of a jet radius, while in the radial direction, the zone width is 1/20 of a jet radius until zone number 192, after which the zone widths are stretched by 2% per zone. This gives a resolution of 20 zones across the radius of the filled jet, and 10 zones across the width of the hollow jets. This resolution is comparable to that used in previous jet simulations; NWS83, NWS84, and LPMB88 use 15 grid zones across their filled jets. KM88 use several resolutions up to 100 zones across the jet radius. The figures shown in this paper include the full extent of the computational region.

We employ outflow boundary conditions except at the orifice and on the symmetry axis. This is clearly appropriate for the outer radial boundary and the downstream axial boundary, but one can select either a reflecting or an outflow condition on the upstream axial boundary. We choose an outflow boundary condition, because in our picture of the model system, the computational region is sufficiently far from the source of the jet that there is no interaction between this jet and the counter jet on the opposite side. The question of which boundary condition is appropriate for jet simulations has been an issue in the past; the choice of one or other of these boundary conditions has demonstrable qualitative effects upon the resulting jet (KM88).

We calculate a pair of standard cylindrical filled jets ($M_j = 6.0$ and $\eta = 1.0$ and 0.1) for comparison with simulations by other authors (NSW83; NWS83; NWS84; LPMB88; KM88), and to provide a baseline against which to compare the results

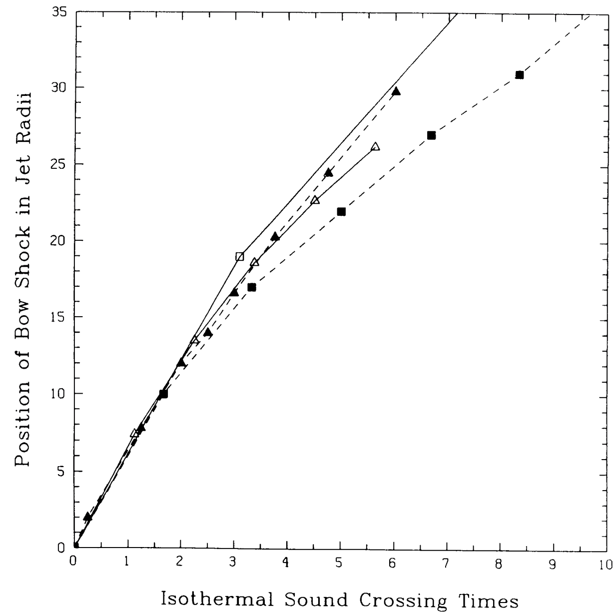

FIG. 1.—Position of bow shock for four different jet calculations. NSW85; $M_j = 6$, $\eta = 0.1$, 15 grid zones across jet (*solid line and open squares*); LPMB88: $M_j = 6.1$, $\eta = 0.1$, 15 grid zones across jet (*dashed line and solid squares*); KM88: $M_j = 6.0$, $\eta = 0.1$, 40 grid zones across jet (*dashed line and solid triangles*); this work: $M_j = 6.0$, $\eta = 0.1$, 20 grid zones across jet (*solid line and open triangles*).

of the hollow jets. While the various jets are qualitatively similar in terms of gross morphology (shock structure, vortex shedding), evolution, and stability, there are differences between them. For example, the rate of advance of the bow shock varies (see Fig. 1). The bow shock's advance is controlled by the size of the working surface (see eq. [3.3]), which in turn depends on the size of the cocoon and the formation of vortices at the head of the jet—in short, it is sensitive to all of the details of the jet's structure.

The effect of boundary conditions and numerical resolution on the propagation of jets is studied in KM88. They show that these considerations have significant quantitative effects in the locations of the bow shock and working surface, as well as the structure and vorticity of the cocoon. For example, the development of structure in the cocoon, and hence the effective area of the working surface, depends primarily on the shedding of vortices at the head of the jet. The production of vorticity in the codes will clearly depend on initial conditions, differences in algorithm (numerical viscosity), and boundary conditions. The similarity of the cocoon and shock structures at late times in comparably resolved simulations suggests that the observed differences may be due to initial transients rather than inherent numerical viscosity. Note that all the compared results were obtained with second-order, monotonic schemes, that, although different in implementation, can be expected to have roughly the same numerical diffusion. With the exception of the LPMB88 results, the jets initially show little or no structure and advance ballistically into the ambient medium; only when the flow begins to exhibit complex structures does the jet slow down. The hydrodynamic jet of LPMB88 has considerably more vortical structure in its cocoon and a correspondingly smaller velocity for the bow shock. Their jets are closer in appearance to the reflecting boundary condition runs of KM88, which also have more substantial cocoons and slower average bow shock velocities. The implication of these comparisons is that simulations will differ not only in the exact properties of the flow structure at any one time, but even in certain gross properties such as the position of the bow shock and working surface.

While we do not want to minimize problems of resolution, numerical methods, boundary conditions, and initial data, we believe that these simulations do provide valuable insights into the basic physics of supersonic hydrodynamic jets. All the simulations discussed here agree on the basic morphology and stability properties of the jets. Comparative studies such as that of KM88 delineate the limits of applicability for the present numerical work. Further code comparison and validation is desirable, but the jets seem to be a poor test bed for doing detailed comparisons of numerical techniques. The flow patterns are nonstationary and the details of the flow continually feed back into the jet to determine properties such as the rate of advance. The differences between the simulations highlight the need for well-defined, inherently two-dimensional test problems in numerical hydrodynamics.

III. JET KINEMATICS AND DYNAMICS

While the evolution of a hydrodynamic jet is not amenable to analytic treatment, there are a number of kinematic arguments that give approximate expressions for the behavior of certain large features of the jet. The analysis is based upon nothing more than conservation laws, yet it provides a reasonable understanding of the macroscopic properties of the jet.

We begin by relating the advance of the jet to the rate at which it transfers momentum to its surroundings through the simple requirement of momentum balance in the rest frame of the working surface of the jet. Equating the momentum flux in the jet with the ram pressure of the ambient gas yields

$$A_j[\rho_j(v_j - v_w)^2 + P_j] = A_w(\rho_a v_w^2 + P_a) , \tag{3.1}$$

where A_j and A_w are the cross sectional areas of the jet and the working surface. The pressure terms can be neglected in high Mach number jets as they represent corrections of order $M_j^{-2} \ll 1$. The velocity of the working surface is

$$v_w \simeq v_j \frac{\epsilon}{1+\epsilon} ; \quad \epsilon \equiv \left(\frac{\rho_j}{\rho_a} \frac{A_j}{A_w}\right)^{1/2} , \tag{3.2}$$

or, in terms of the Mach number of the working surface relative to the sound speed in the ambient medium,

$$M_w = M_j \left(\frac{A_j}{A_w}\right)^{1/2} \frac{1}{1+\epsilon} \tag{3.3}$$

(NW85; LPMB88). A jet can be decelerated either by reducing its density or by increasing the size of the working surface. Using the Mach number rather than the velocity of the jet to parameterize the data insures that the primary variable controlling the rate of advance is the relative areas of the jet and the working surface.

We have no *a priori* way of computing the area of the working surface in the actual jets beyond $A_w \gtrsim A_j$. For filled jets, A_w is approximately given by the radii of the ring shock at the head of the jet (LPMB88). Since even for filled jets, the ring shock is not a stationary feature of the flow, the rate of advance of the jet is not steady, and it depends on the details of the flow at any time.

In the hollow cylindrical jets, if the ratio of jet thickness to average radius is fairly large ($\Delta R/\bar{R} \sim 1$), the jet will form a composite bow shock from the axis to the exterior of the jet, whereas if the ratio is small ($\Delta R/\bar{R} \ll 1$), the jet will form an annular bow shock. In either case, the total area of the effective working surface will be significantly larger than that of the equivalent filled cylindrical jet. The case we examine has $\Delta R/\bar{R} = 0.5$, so that we expect the momentum transfer to occur over a region from the axis to the outer edge of the jet, with $A_w \gtrsim 25A_j/16$ (because the outer edge of the jet is at $5R_j/4$). This implies that the rate of advance of the hollow cylindrical jet will be some 50% slower than the equivalent filled jet.

For the conical jets, geometric expansion increases the jet outer radius $R = R_0 + Z \tan\theta$, where R_0 is the initial outer radius of the jet and Z is the axial distance from the orifice. If the thickness of the jet remains roughly constant, the area of the jet will increase with R. One important consequence of this is that the input momentum flux will be spread over an *increasing* area. The Mach number of the working surface eventually becomes subsonic when the geometric dilution of the momentum flux prevents the jet from driving the ambient material out of its path. At this point, we can think of the jet as having "stalled." Neglecting the density ratio, this distance is simply the point where

$$A_w = M_j^2 A_j , \tag{3.4}$$

where M_j is the initial Mach number of the jet.

A crucial question is whether the area working surface grows proportional to R, corresponding to momentum transfer over an annulus of fixed width about the jet, or proportional to R^2, corresponding to momentum transfer over an annulus with a linearly increasing width. This must depend on how the area of the jet changes as it evolves and on the stability of the jet's channel. For the cylindrical geometries, both hollow and filled, the cross section should remain approximately constant; the jet may wiggle, waggle, and wobble, but it remains a coherent flow directed along the axis. How does the width of the conical jets vary with R? Does the thickness of the jet compensate for or enhance the geometric effects? It seems unlikely, in the absence of significant cooling, that the jet could become narrower, because lateral compressions will generate shocks and hence compensating pressure, in a supersonic flow. This would tend to make any substantial constriction a transient rather than a steady state effect. However, because our resolution across the conical jets is rather low (10 zones at the inlet), we probably cannot completely rule out such a jet constriction. For the jet to become progressively thicker, internal pressure would have to be generated by shocks faster than the pressure decrease from geometric expansion.

We turn then to a consideration of the internal jet dynamics as characterized by the changes in the jet cross sectional area A_j, average density ρ_j, and average Mach number M_j. These are related by the conservation of mass flux along the body of the jet,

$$\rho_j v_j A_j = \text{constant} , \tag{3.5}$$

and conservation of energy along flow lines

$$\frac{1}{2}\rho_j v_j^2 + \frac{\Gamma P_j}{\Gamma - 1} = \text{constant} , \tag{3.6}$$

We do not know what the evolution of the entropy in the jet will be, but the gas has only a few options. It can shock and increase its entropy, or it can evolve at constant entropy. From studies of filled jets, we know that the gas shocks and then expands adiabatically to return to pressure equilibrium. We can ask how the jets evolve in two limits: constant entropy and constant pressure. In these two cases, the density evolves with Mach number as

$$\begin{aligned} \rho &= \rho_0 \left[\frac{(\Gamma-1)M^2+2}{(\Gamma-1)M_0^2+2}\right]^{-1/(\Gamma-1)} & S &= \text{constant}, \\ \rho &= \rho_0 \left[\frac{(\Gamma-1)M^2+2}{(\Gamma-1)M_0^2+2}\right] & P &= \text{constant}. \end{aligned} \tag{3.7}$$

A similar set of equations can be written to relate the cross sectional area of the jet and the Mach number

$$\begin{aligned} A &= A_0 M_0 \left[\frac{(\Gamma-1)M^2+2}{(\Gamma-1)M_0^2+2}\right]^{-(\Gamma+1)/2(\Gamma-1)} & S &= \text{constant}, \\ A &= A_0 M_0 \left[\frac{(\Gamma-1)M_0^2+2}{(\Gamma-1)M^2+2}\right]^{1/2} & P &= \text{constant}. \end{aligned} \tag{3.8}$$

The first of these assumptions describes the local postshock behavior of the jet gas, while the second should more closely model the overall evolution of the jet. In the case of the filled jets, internal shocks gradually increase the entropy. One consequence is that the cocoon is hotter and lighter than the jet (NW85). The conical jets have the additional geometrical complication of a constantly increasing cross sectional area. If the entropy of the jet were constant as the area increased, the Mach number and jet density would drop. However, if the ambient medium has sufficient inertia, the jet *cannot* freely expand. It will be shocked and more or less brought into pressure balance. If we assume that the conical jet evolves at a constant pressure and jet thickness ΔR, so that the cross sectional area increases linearly with radius R, the internal Mach number of the jet decrease as $M_j(R) = M_0(\bar{R}_0/R)^{1/2}$. This is essentially the same condition as (3.4), except that here we are concerned with the conservation of momentum within the jet and not with its transfer to the surrounding gas.

From this analysis, we see that a conical jet will, in the absence of significant cooling, evolve toward lower Mach numbers. As its Mach number decreases, the jet will become unstable to local "kink" modes, developing ripples with wavelengths ranging from the jet thickness ΔR to the distance from the axis R. These will locally resemble the instabilities of slab jets studied by NW85, so the criterion for the onset of the instability is probably similar ($M_j \lesssim 1 + \eta^{1/2}$), although we have not attempted to work out the exact condition (see also Hardee and Norman 1988; Norman and Hardee 1988). Regardless, the jet will eventually become subsonic and stall, or disrupt as the jet Mach number drops below the stability threshold.

The preceding discussion has assumed that the jet is surrounded by a constant pressure ambient medium. However, the properties of the medium in which the jet propagates can be just as complicated as those of the jet itself, significantly affecting jet evolution. Previous studies have found that the dynamics of filled jets are affected by self-interactions with a cocoon of spent gas. While the jet is injected in pressure equilibrium with the ambient medium, it propagates through a cocoon that not only has an unknown pressure, but is also in motion (*supersonic* motion in some regions). The initial data, therefore, are not completely consistent with the subsequent physical conditions at the inlet. If the jet is injected into a higher pressure medium characterized by pressure $P > P_j$, then (assuming a fixed cross sectional area and pressures small compared to the jet ram pressure) the jet will quickly change its Mach number

$$M_j \to M_j\left(\frac{P_j}{P}\right)^{1/2}, \tag{3.9}$$

to come into pressure equilibrium with its surroundings. This makes it extremely difficult to inject high–Mach number jets in a fully self-consistent manner; the jets will shock and reduce their internal Mach number to achieve pressure balance with the cocoon. This leads to the "inlet shocks" that extend from the edge of the jets at the inlet to a Mach disk approximately $M_j R_j$ downstream. This is not a problem with the lower Mach number $M_j = 6$ jets, but it does seem to complicate the evolution of the higher Mach number $M_j = 12$ jets. Typically, the cocoon pressure is roughly twice the ambient pressure, so that the jet Mach number can drop by nearly 50% at the inlet shock.

As with the jet, we can do some analysis of the cocoon through the use of conservation laws. Details are more difficult to obtain, because the cocoon is an amorphous structure, but some general relationships should hold. The cocoon is formed when the injected gas reaches the end of the jet and is decelerated by a strong shock. In fact, the gas flows through a series of terminal shocks which increase the pressure and entropy. The pressure then equilibrates (to first approximation) through adiabatic $P\,dV$ work. If we model this by passing the jet gas through a strong shock characterized by the Mach number of the jet and then reducing the gas pressure to that of the ambient medium through adiabatic expansion, the resulting gas density is

$$\rho_f \simeq \alpha \rho_j M_j^{-2/\Gamma}, \quad \alpha \simeq \frac{\Gamma+1}{\Gamma-1}\left(\frac{2\Gamma}{\Gamma+1}\right)^{-1/\Gamma}, \tag{3.10}$$

where for a $\Gamma = 5/3$ gas, $\alpha \simeq 3.5$. This roughly matches the densities in the cocoon (to within a factor of 2 in either direction) away from the cores of supersonic vortices, where the density can be a factor of 10 smaller owing to centrifugal effects. Note that for the conical jets, there is a correction of $(\bar{R}_0/R)^{(\Gamma-1)/\Gamma}$ to the cocoon density, under the assumption that the jet maintains a fixed width and constant pressure as it propagates from the injection radius at $\bar{R}_0$ to the terminal shock at radius R. This follows from equation (3.7).

We can combine the cocoon density and the jet mass flux to estimate the size of the cocoon, assuming that the jet gas does not mix with the ambient gas (at least not initially). We must distinguish, however, between the two cases of an advancing jet and a stalled jet. If we assume for an advancing jet that the cocoon is laid down by the working surface at rest in the "lab" frame, then using equation (3.2), the equilibrium outer radius for the cocoon R_c is

$$\left(\frac{R_c}{R_j}\right)^2 \simeq 1 + \alpha^{-1} M_j^{2/\Gamma} \eta^{-1/2}\left(\frac{A_w}{A_j}\right)^{1/2}, \tag{3.11}$$

where A_w is the area of the working surface. In practice, this should be an upper limit; when using outflow boundary conditions, the cocoon flows back off the grid rather than remaining at rest. Further, the cocoon and the post–bow shock ambient gas will be at a higher pressure than the initial P_a. However, the functional dependence clearly shows the transition to a naked beam for dense jets, and the growth of the cocoon with Mach number. Note that since the size of the cocoon depends on the rate of advance, and hence on the size of the working surface, a hollow cylindrical jet with its larger working surface generates a larger cocoon as compared with a filled jet of the same Mach number and density ratio.

If the jet is stalled rather than propagating, the cocoon inflates a vortex ring at the head of the jet. If we model such a vortex as a toroidal ring with its center at distance R from the axis and radius r_v, the mass of spent jet gas enclosed in the "vortex" is $2\pi^2 R r_v^2 \rho_f$. (Note that we have ignored the dynamics of the vortex.) The torus is inflated by the mass flux of the jet, $A_j \rho_j v_j$. If we allow the torus to grow with fixed R and time-dependent r_v, then the growing torus will start to interfere with the flow of the jet when $r_v \sim R_j$. This defines a vortex formation time (in units of the isothermal sound crossing time t_i)

$$\frac{t_v}{t_i} = 2\pi\alpha\Gamma^{-1/2} M_j^{-(\Gamma+2)/\Gamma} \eta^{1/2} \left(\frac{R}{R_j}\right)\left(\frac{r_v}{R_j}\right)$$
$$\simeq 0.3\eta^{1/2}\left(\frac{M_j}{6}\right)^{-2.2}\left(\frac{R}{R_j}\right)\left(\frac{r_v}{R_j}\right)^2 . \tag{3.12}$$

For the conical jets, we must include the correction to the final density for the increase of jet volume with R, so that at the stalling radius $R \sim M_j R_j$,

$$\frac{t_v}{t_i} \simeq \eta^{1/2}\left(\frac{M_j}{6}\right)^{-1.6}\left(\frac{R}{M_j R_j}\right)^{0.6}\left(\frac{r_v}{R_j}\right)^2\left(\frac{\bar{R}}{R_j}\right)^{0.4} , \tag{3.13}$$

where the latter two results assume a $\Gamma = 5/3$ equation of state. Hence, jets in this Mach number regime periodically shed vortices on time scales of order $t \simeq t_i$. This basic idea of the time scale for vortex shedding applies to both filled and hollow jets. As a consequence, the filled jets advance steadily only when considered on time scales greater than t_i; on shorter time scales, the terminal shock system can slow as vortices are formed and shed at the head of the jet.

IV. NUMERICAL RESULTS

We have carried out a program of numerical experiments that includes a baseline of filled cylindrical jets, a set of hollow cylindrical jets, and a set of hollow cones. The simulations are performed with jet internal Mach numbers $M_j = 6$ or 12, and jet to ambient medium density ratios of $\eta = 0.1$ and 1.0. Table 1 lists the numerical models that have been calculated for this investigation. Contour plots from late times in the simulations are displayed in Figures 2–5. The hydrodynamical behavior of the filled jets is discussed in § II. In this section, we discuss the results for the other geometries.

TABLE 1

MODELS STUDIED IN THE PARAMETER SURVEY

Jet Mach Number	Density Ratio	Jet Geometry
6.0	0.1	Filled cylinder
	0.1	Hollow cylinder
	0.1	Hollow cone
12.0	0.1	Hollow cone
6.0	1.0	Filled cylinder
	1.0	Hollow cylinder
	1.0	Hollow cone
12.0	1.0	Hollow cone

a) Hollow Cylinders

We consider first the geometry of the hollow cylindrical jet. As described in § II, the area of the jet orifice is chosen to be the same as that of the filled jet, so that both geometries begin with the same total momentum flux. From Figures 2–5, it is apparent that hollow cylindrical jets are, in some sense, similar to the filled jets. They are approximately stable and propagate like extremely blunt filled jets. However, the hollow cylindrical jets show several qualitative departures from the behavior of the filled jets. There are three significant differences: (1) the working surface is blunter, (2) the cocoon is larger, and (3) the cocoon-jet interactions are more complex.

The first two of these differences can be understood by considering the working surface at the head of the hollow cylinder. Although the hollow cylinder's cross sectional area is the same as the filled jet, the area of its working surface is significantly larger, extending at least from the jet's outer surface to the axis. This manifests itself as a lower rate for jet propagation (see Figs. 6–7; eq. [3.2]). Relative to the similar filled jet, the $M_j = 6$, $\eta = 1.0$ hollow jet takes 30% longer to reach the edge of the grid, and the $M_j = 6$, $\eta = 0.1$ hollow jet takes 60% longer. Slower propagation means more spent jet gas is forced into the cocoon per unit length of the jet, resulting in a larger cocoon (see eq. [3.11]). Even the $M_j = 6$, $\eta = 1.0$ case, which is a "naked beam" filled jet, develops a cocoon in the hollow geometry.

Since we observe larger cocoons in the hollow cylindrical geometry, it is not surprising that the cocoon-jet interactions are more complex than in the filled jet. One important feature is the "plug" of high-pressure gas that forms at the head of the jet. In the filled jets, the leading plug of shocked material causes the outward deflection of the jet along an oblique shock (LPMB88). In the hollow jets, it is larger, and as a result, the jet undergoes a dramatic outward "flaring" along the surface of the plug that creates large supersonic vortices in the cocoon. Initially, the plug is composed of shocked ambient gas, but later it contains material from weak, inwardly shed vortices drifting backward into the jet. These vortices are suppressed by the small volume interior to the jet and by the forward motion of the plug. Except for the plug, the interior region is filled with shocked *ambient* gas, and the cocoon is restricted to the exterior of the jet.

The supersonic vortices in the cocoon of the filled jets trigger the formation of the now-familiar crossed shock patterns in the jet. In the hollow cylindrical geometry, the jet is perturbed by both the vortices of the cocoon and by pressure fluctuations in the shocked ambient gas along the axis; in general, these two sources of perturbations will not act coherently. In our simulations, the cocoon is the dominant source of perturbations away from the head of the jet. This results in a partial focusing of the jet channel roughly midway between the inlet and the working surface of the jet, where the largest vortex impinges on the surface of the jet channel (see Fig. 8). The material on the interior is compressed by the inward motion of the jet, eventually raising the pressure sufficiently to move the jet away from the axis. The competition between the two forces drives oscillations in the position of the jet's channel (Fig. 9).

As a consequence of this complex interaction, the "simple" shock structure of the filled jets is lost (see Fig. 8). Although there are a series of crossed shocks on the axis, these are formed in response to the pinching action of the jet on the interior gas. The jet itself does not have a well-defined shock structure. The wall of the hollow cylindrical jet has no enforced geometric symmetry, and this permits more irregular behav-

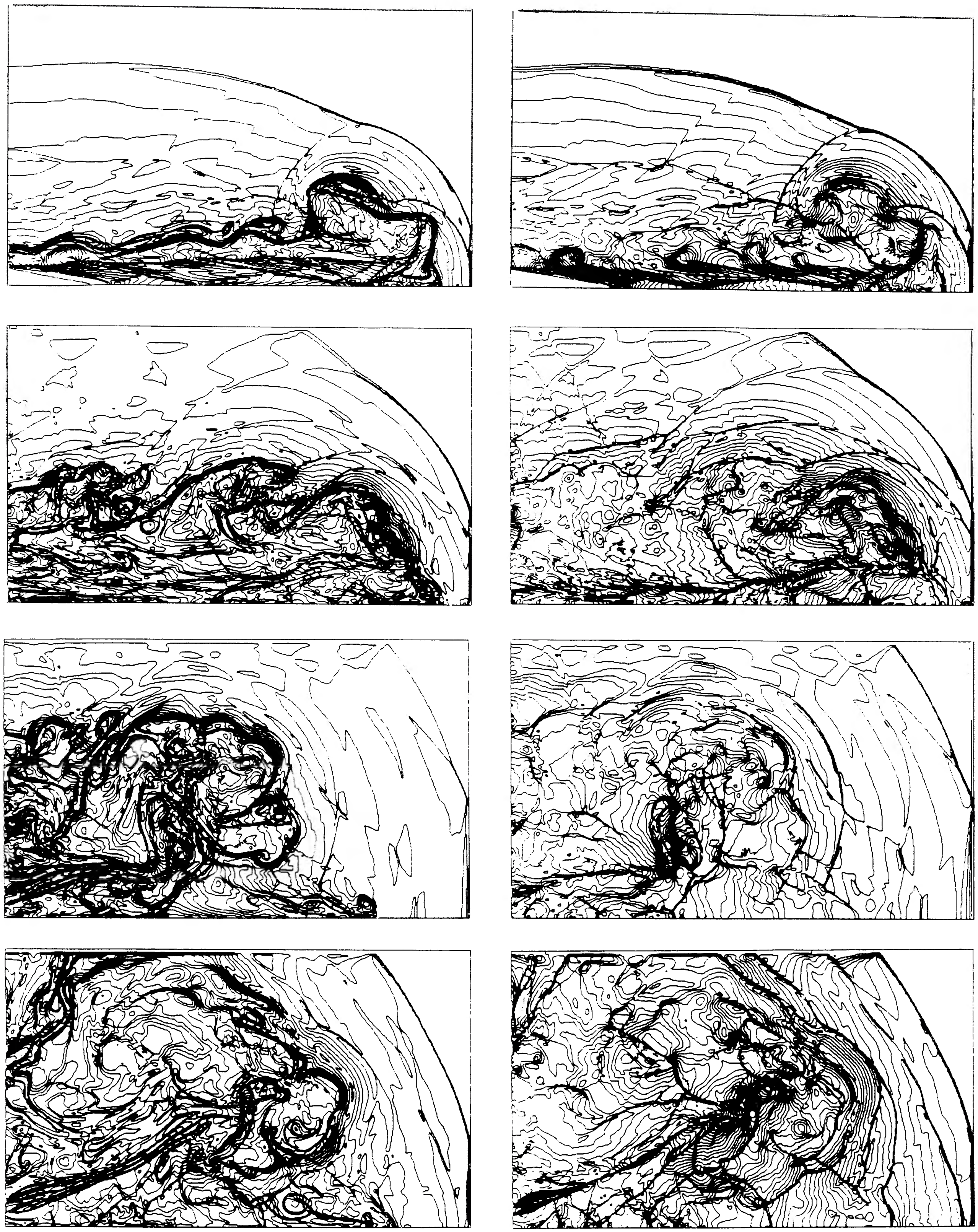

FIG. 2.—Density and pressure contours of the density contrast $\eta = 0.1$ jets examined in this study at their final time level, where the bow shock is near or slightly past the downstream boundary. Thirty contours distributed uniformly in the logarithm of the density and pressure are displayed. On the right is the density, and on the left is the pressure. The cases are (from top to bottom) the filled, cylindrical, and conical $M_j = 6$ jets, and the conical $M_j = 12$ case. Time levels of the contours are $t/t_i = 5.6, 9.0, 11.3$, and 6.8, respectively.

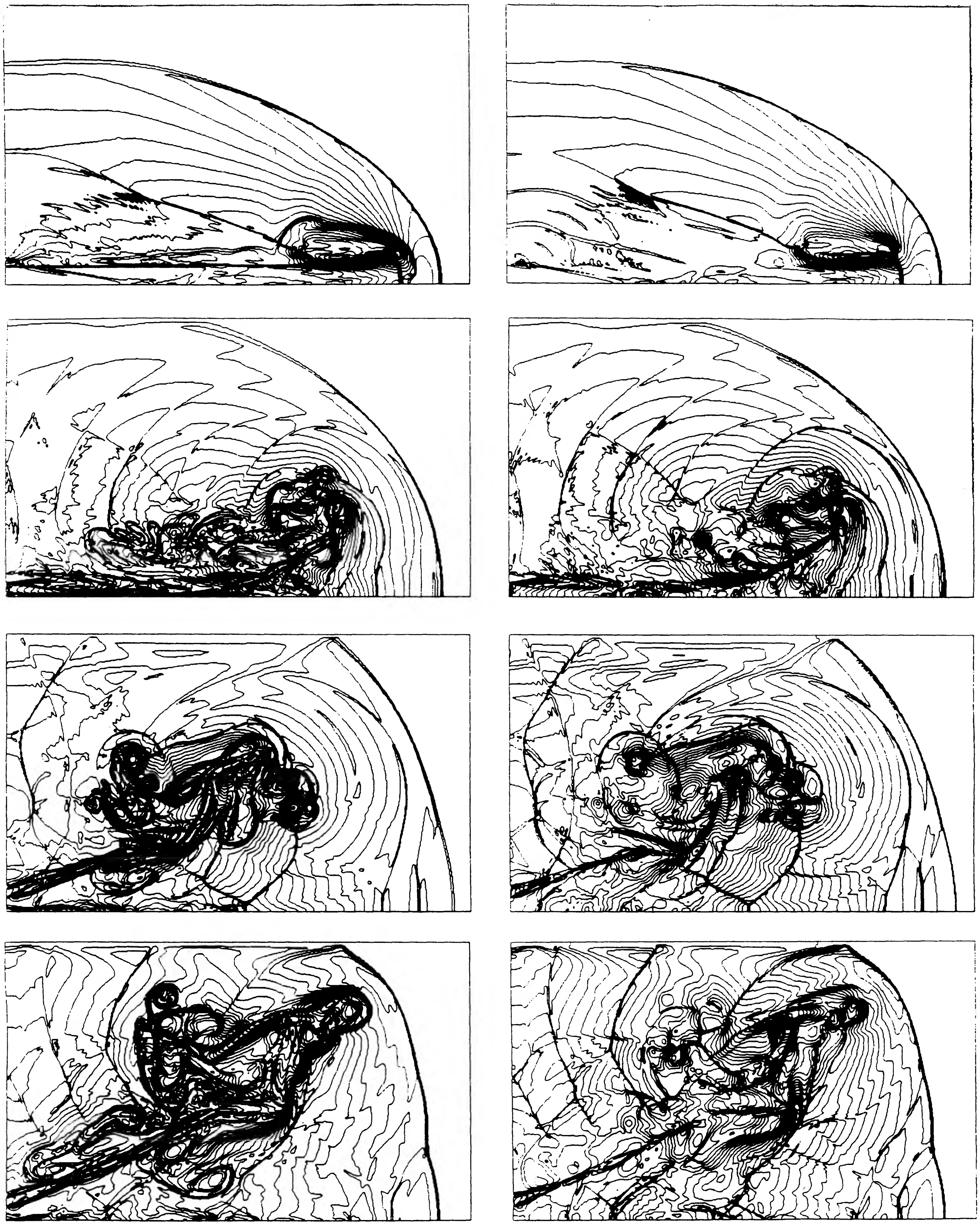

FIG. 3.—Density and pressure contours of the density contrast $\eta = 1.0$ jets examined in this study at their final time level, where the bow shock is near or slightly past the downstream boundary. Thirty contours distributed uniformly in the logarithm of the density and pressure are displayed. On the right is the density, and on the left is the pressure. The cases are (from top to bottom) the filled, cylindrical, and conical $M_j = 6$ jets, and the conical $M_j = 12$ case. Time levels of the contours are $t/t_i = 6.8, 9.0, 11.3$, and 6.8, respectively.

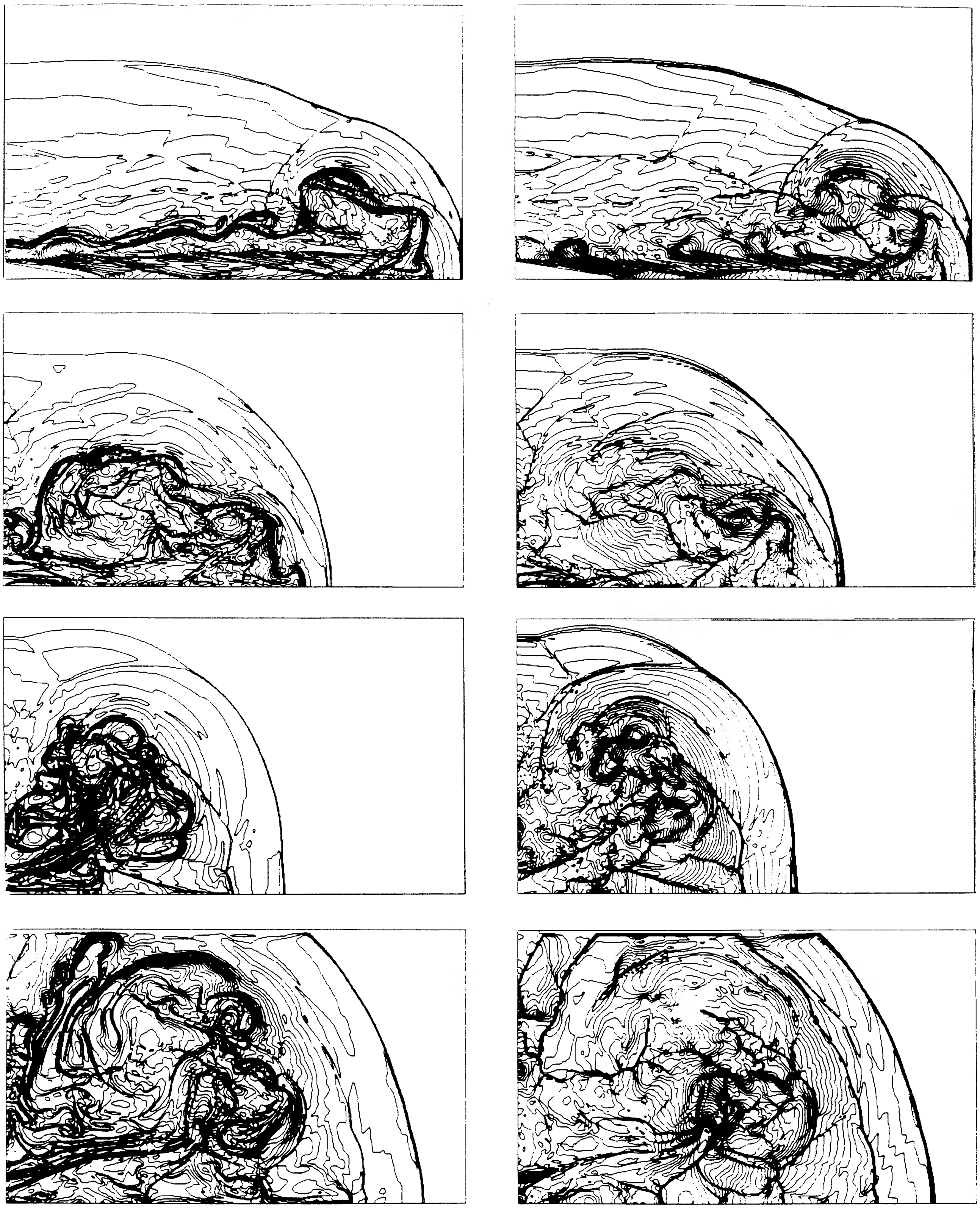

FIG. 4.—Density and pressure contours of the density contrast $\eta = 0.1$ jets examined in this study at the same time level $t/t_i = 5.6$. Thirty contours distributed uniformly in the logarithm of the density and pressure are displayed. On the right is the density, and on the left is the pressure. The cases are (from top to bottom) the filled, cylindrical, and conical $M_j = 6$ jets, and the conical $M_j = 12$ case.

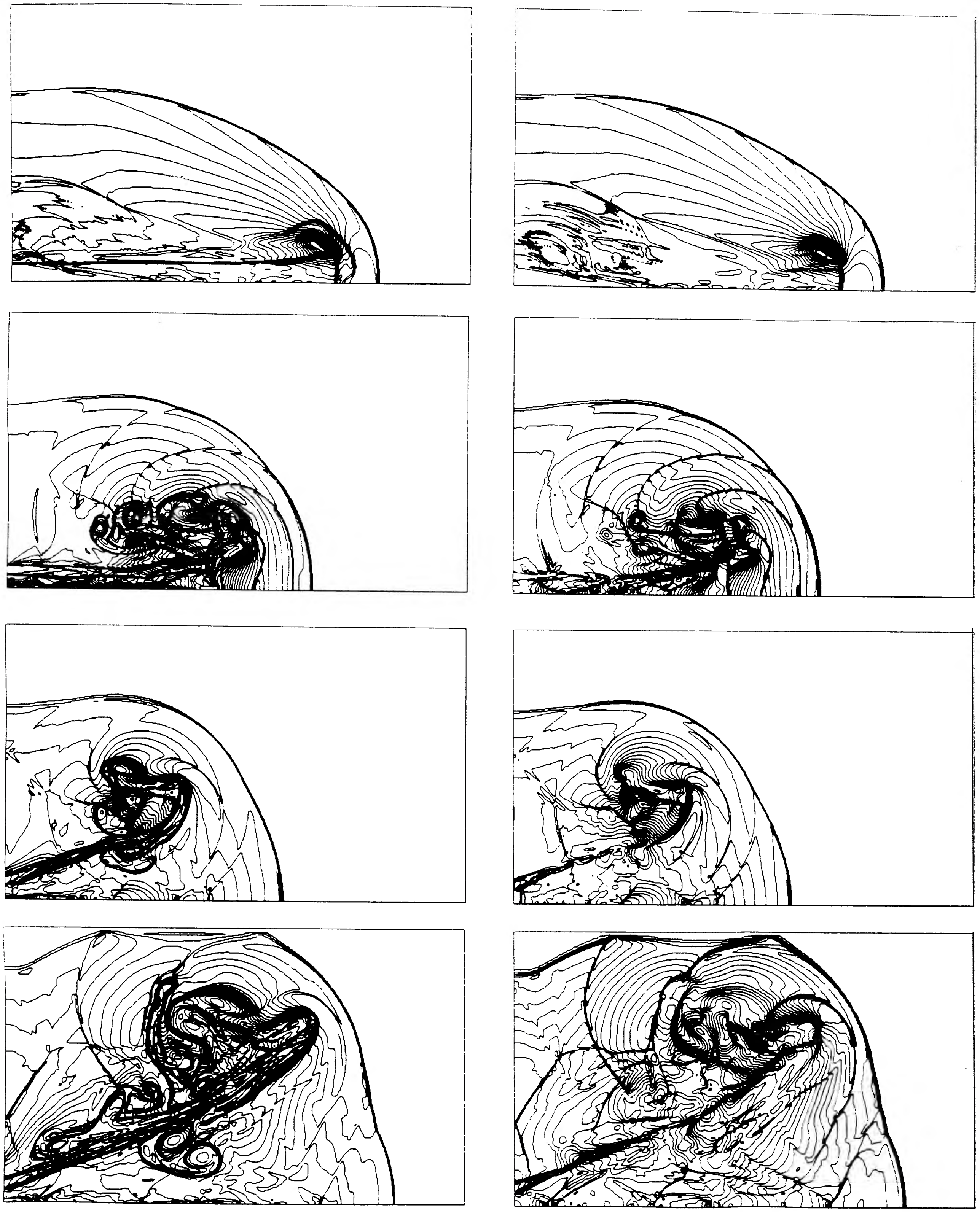

FIG. 5.—Density and pressure contours of the density contrast $\eta = 1.0$ jets examined in this study at the same time level $t/t_i = 6.8$. Thirty contours distributed uniformly in the logarithm of the density and pressure are displayed. On the right is the density, and on the left is the pressure. The cases are (from top to bottom) the filled, cylindrical, and conical $M_j = 6$ jets, and the conical $M_j = 12$ case.

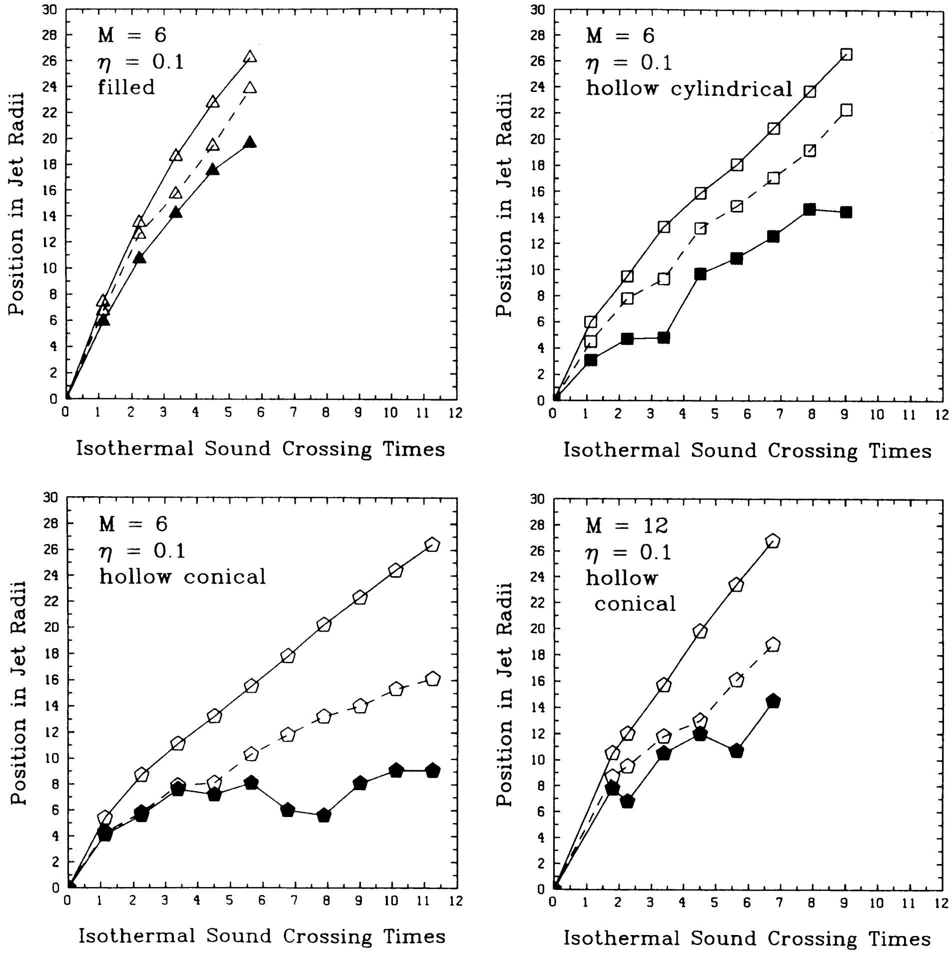

FIG. 6.—Position of the bow shock (*open symbol and solid line*) contact discontinuity (*open symbol and dashed line*), and terminal shock (*filled symbol and solid line*) for the four cases with density ratio $\eta = 0.1$.

iour. In this sense, a section of the hollow cylinder resembles a slab jet (NW85; Hardee and Norman 1988; Norman and Hardee 1988), which can develop large kink mode perturbations. Because the Mach number of the jet is sufficiently supersonic to avoid the normal criterion for the onset of instability ($M_j \lesssim 1 + \eta^{1/2}$), the strong perturbations can excite large "kink-like" oscillations without the jet becoming catastrophically unstable. If the Mach number of the jet is reduced to the transonic regime, the oscillations will grow rapidly and disrupt the jet.

b) Conical Jets

While the hollow cylindrical jets possess some superficial resemblance to the filled jets, the hollow conical jets have remarkably different properties. The most dramatic of these is that *hollow conical jets do not propagate.* In each case, the head of the jet reaches a limiting distance at which it stalls. For the Mach 12 models, the $\eta = 1$ jet stalls at a distance of $14R_j$, and the $\eta = 0.1$ jet stalls at $12R_j$. For the Mach 6 jets, these distances are $8R_j$ and $6R_j$. (See Figs. 6 and 7).

The geometric increase in both the interior volume of the cone and the cross sectional area of the conical jet must account for this effect. We observe that the jet width, ΔR, does not change much over the length of the jet, so the cross sectional area of the jet increases proportional to R. The stalling radius seems to increase linearly with the initial Mach number which suggests, by the analysis in § III, that the effective working surface grows with R^2. The effective working surface must extend over the entire region interior to the jet instead of being a thin annulus centered on the jet. Equation (3.8), which relates the jet's cross sectional area to its Mach number, requires that the jet thickness must increase with R if the stalling distance is to be linear in the Mach number. Because this does not agree with the observed behavior of the jet, the stalling mechanism apparently depends more on momentum transfer to the external gas than on the evolution of the parameters of the jet.

We find a weak dependence of stalling radius on the density parameter η. The sense of this dependence is not consistent with the simple theory (eq. [3.2]); in our simulations, lower density ratios stall at smaller distances. The result is consistent with the presence of higher pressure cocoons surrounding low-η jets. Recall that the effective initial Mach number is reduced by the presence of a higher pressure cocoon (eq. [3.9]).

A second important difference between the conical and filled jets is that the conical jets are very unsteady flows. It is not possible to demonstrate fully the degree to which the conical jets depart from a steady flow pattern with a series of contour plots. We did not fully appreciate the nature of the flow until we generated a computer-animated film of the propagation of

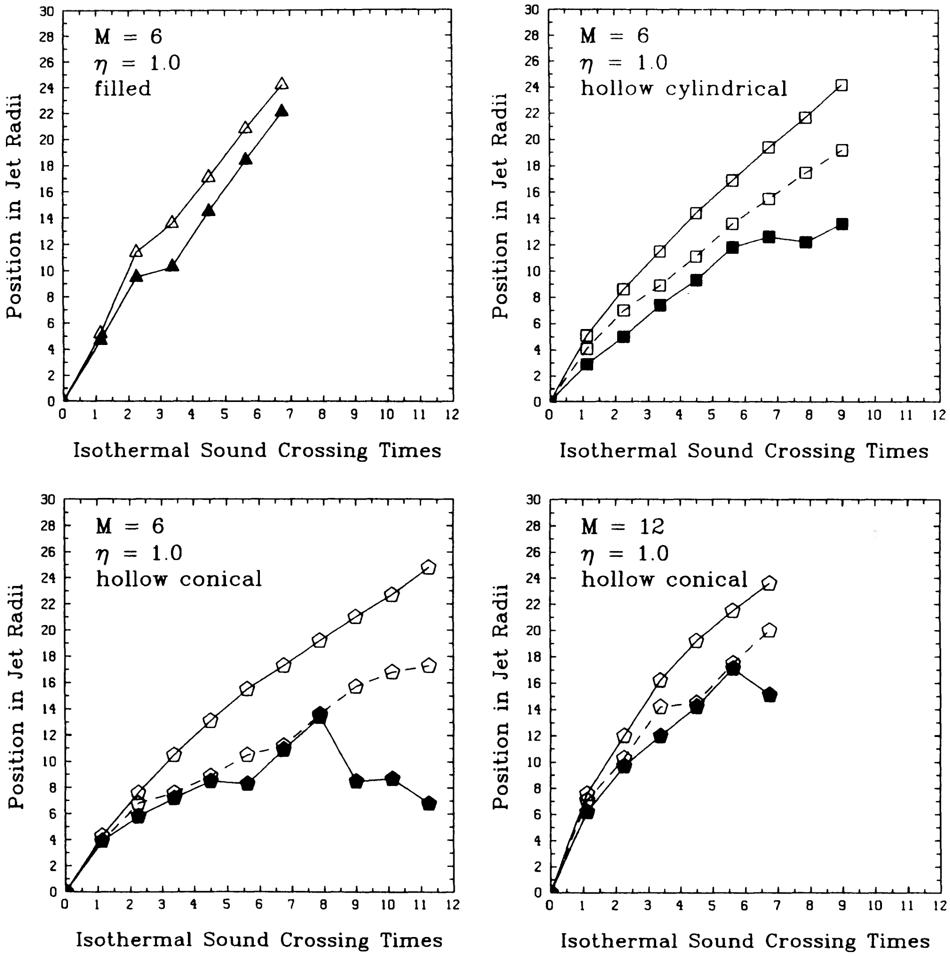

FIG. 7.—Position of the bow shock (*open symbol and solid line*) contact discontinuity (*open symbol and dashed line*), and terminal shock (*filled symbol and solid line*) for the four cases with density ratio $\eta = 1.0$. Note that in the cylindrical $M_j = 6$ case, the contact discontinuity and the terminal shock are essentially coincident.

conical jets, and the descriptions of the flow patterns in this section are derived mainly from observing these animated sequences.

When the conical jet is first injected into the grid, shock waves are driven into the interior of the cone. The bow shock directed towards the interior is focused and strengthened by the symmetry about the axis. Moreover, unlike the bow shock on the exterior of the cone, the pressure built up behind the shock wave can be reduced only by expanding along the axis or by pushing the jet away from the axis. The shock-generated pressure gradient immediately deflects the jet out from the axis. After propagating several jet radii, this deflection has become large (nearly perpendicular to the axis at the head of the jet), and the head of the jet rolls off into large vortex. The accumulation of cocoon gas in these vortices, and the dynamical pressure from the still supersonic cocoon gas impinging on the outer surface of the jet, provides compensating pressure that gradually pushes the jet back toward the axis. This in turn recompresses the gas interior to the jet, raising the pressure to the point where the jet is again driven outward.

In effect, the jet acts as a "wall" separating the interior and exterior gas. Pressure balance is maintained only by deflecting this jet wall. The ambient exterior gas is able to expand away from the jet toward the grid boundary and is thus not able to provide the needed confining pressure. This role falls to the cocoon gas, and the time-dependent dynamics of the hollow jet are dominated by perturbations in the cocoon, particularly by the action of the vortices generated at the head of the jet. As for the shocks generated in the interior of the cone, they are directed out along the axis by the jet wall. These shocks catch up with the bow shock and help drive it outward along the axis. The result, however, is an extremely flat bow shock that has no resemblance to the "ears" of W50 (Fig. 10).

These changes in the pressure gradients, both inside and outside the jet, lead to continual vortex production at the head of the jet, and cause the flow to be extremely nonsteady (Fig. 11). The dramatic radial oscillations cause the momentum flux of the jet to be "sprayed" over the entire region interior to the precession cone. Thus, these oscillations contribute to the stalling process by insuring that the jet momentum is distributed over a substantially larger area than the thin shell about the precession cone. This accounts for the R^2 growth in the effective working surface. Similar radial oscillations were observed in the cylindrical jets, but they are larger for the conical jet as the geometry makes the restoring forces weaker.

The vortices are usually created with the sign natural to the side of the jet on which they are formed. The time scale for their formation and shedding is roughly in accord with the simple arguments of § III. The vortices frequently interfere with the working surface, either by becoming so large that they

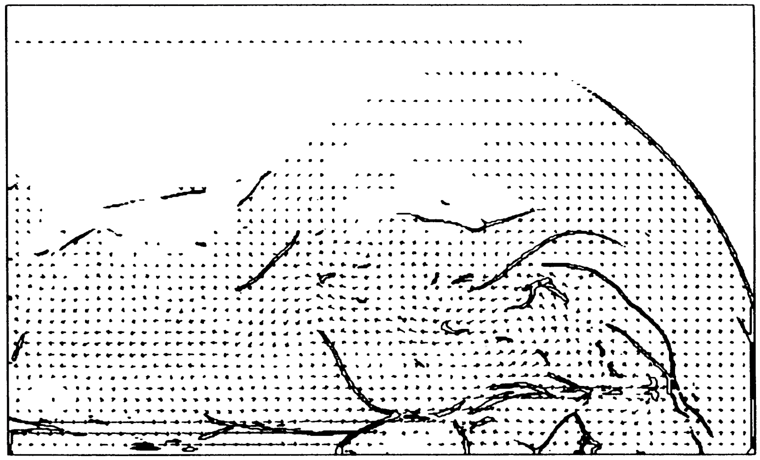

FIG. 8*a*

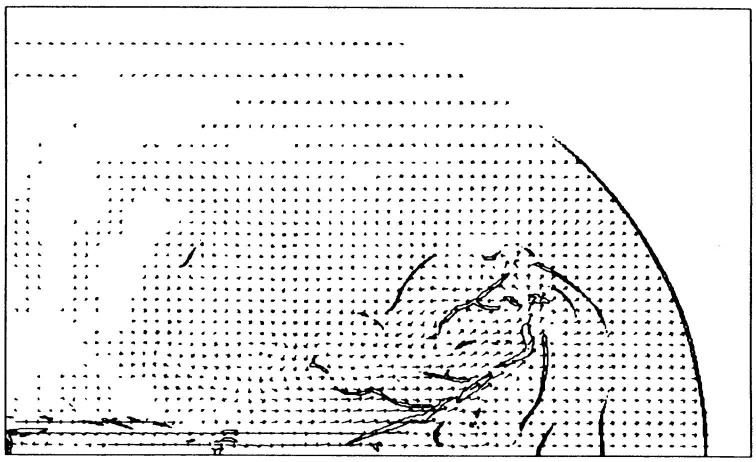

FIG. 8*b*

FIG. 8.—Velocity and shock structure for the two hollow cylindrical cases at the final time slice, $t/t_i = 9.0$. The $M_j = 6$, $\eta = 0.1$ case is shown in (*a*), and the $M_j = 6$, $\eta = 1.0$ case is shown in (*b*). Vectors indicate direction and magnitude of the fluid velocity, with the length proportional to the square root of the velocity. Only every eighth velocity vector is shown in each direction. Contours are of large negative $\boldsymbol{div} \cdot \boldsymbol{v}$, indicating the position of shocks.

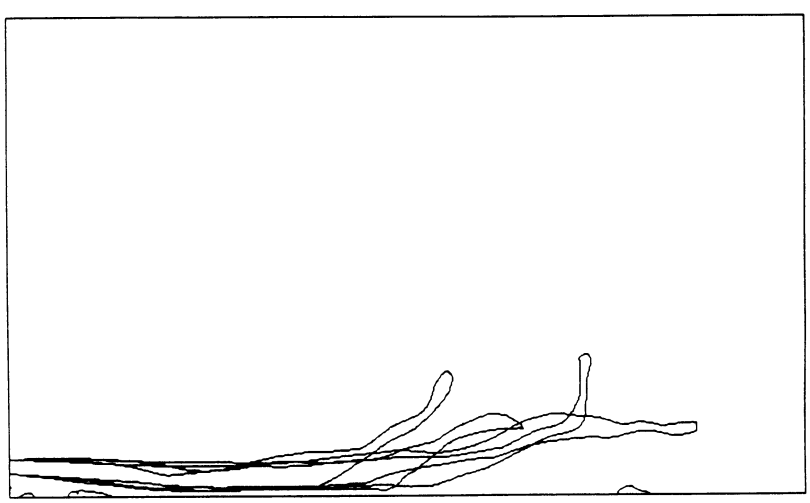

FIG. 9.—Position of the jet channel for the $M_j = 6$, $\eta = 0.1$ hollow cylindrical jet, showing its varying position with time. Channel is defined by the region in which the total gas velocity is greater than 60% of the initial jet velocity. Contours are shown as $t/t_i = 5.6$, 6.8, 7.9 and 9.0. Inward pinching of the jet channel is clearly visible.

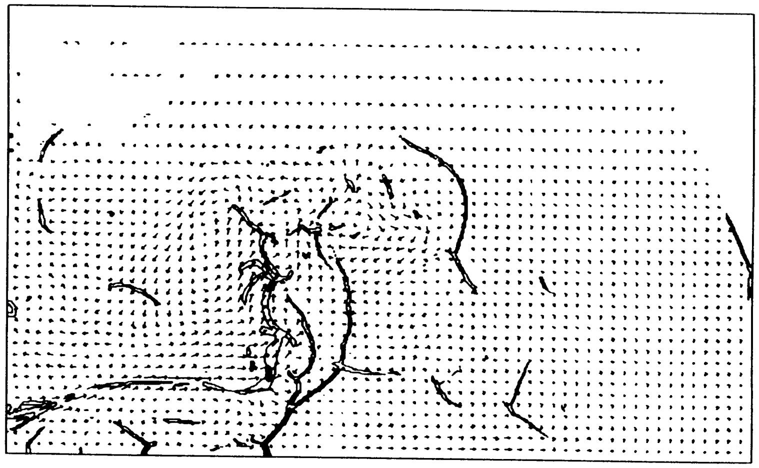

FIG. 10*a*

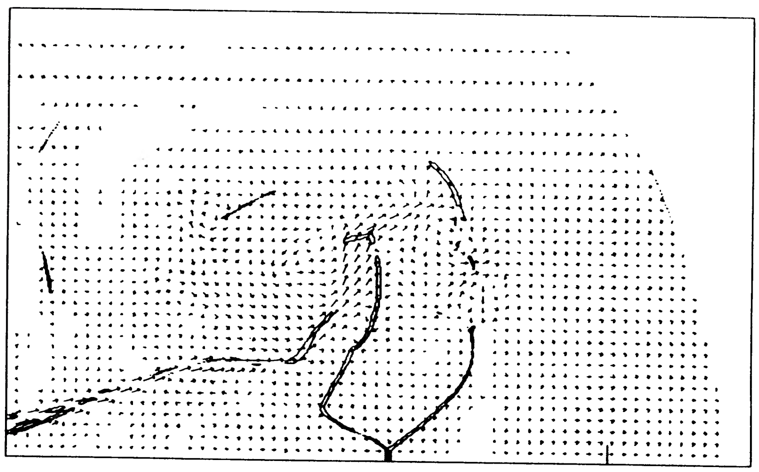

FIG. 10*b*

FIG. 10.—Velocity and shock structure for the two $M_j = 6$ hollow conical jets at the final time slice, $t/t_i = 11.3$. The $M_j = 6$, $\eta = 0.1$ case is shown in (*a*), and the $M_j = 6$, $\eta = 1.0$ case is shown in (*b*). Vectors indicate direction and magnitude of the fluid velocity, with the length proportional to the square root of the velocity. Only every eighth velocity vector is shown in each direction. Contours are contours of large negative $\boldsymbol{div} \cdot \boldsymbol{v}$, indicating the position of the shocks.

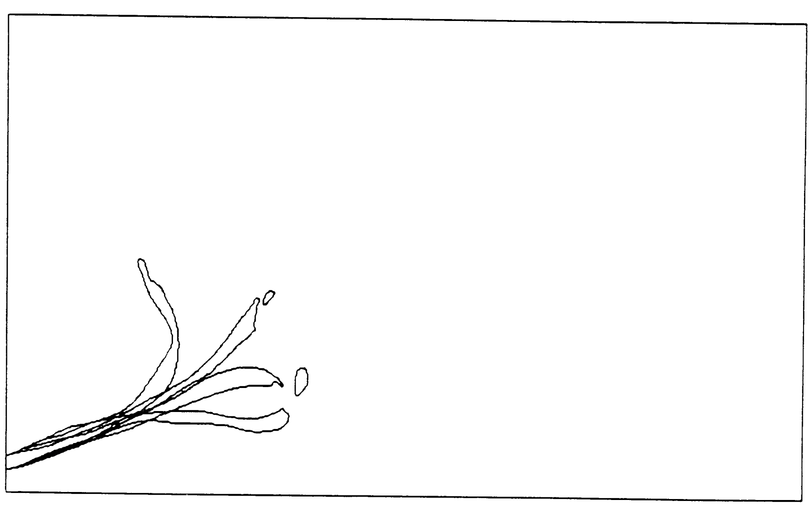

FIG. 11.—Position of the jet channel for the $\eta = 0.1$ hollow conical jet showing its varying position with time. Channel is defined by the region in which the total gas velocity is greater than 60% of the initial jet velocity. Contours are shown at $t/t_i = 7.9, 9.0, 10.1$ and 11.3. Radial oscillations in the jet channel are clearly visible.

"smother" the head of the jet or by propagating into the path of the jet. Large vortices do not persist inside the cone. Once outside the jet, the vortices slowly drift backward toward the upstream boundary. Occasionally, the jet is able to "tunnel" through a vortex at its head and send a brief pulse of the highly supersonic jet gas through the cocoon. When this gas reaches the contact discontinuity separating the cocoon from the shocked ambient gas, it drives a shock wave outward through the medium. This leads to a quasi-periodic system of shock waves traveling outward along the axis behind the bow shock, and the slow forward motion of the contact discontinuity seen in Figures 6–7.

The internal properties of the jet are monitored through the use of tracer particles. Along the jet, the Mach number decreases rapidly both due to shocks and to the geometric diulution of the jet. Since the velocity remains roughly constant, the jet density drops linearly with radius. The Mach number drops even faster, due to shock waves that keep the jet pressure more or less in equilibrium with its surroundings. We know that if the jet Mach number drops far enough, the jet becomes unstable to kinking modes, and the large oscillations of the jet provide an abundance of perturbations to drive the instability. It is difficult, however, to determine whether the jet Mach number drops sufficiently far while the jet can be characterized as a coherent flow structure. The jet disrupts into a series of vortices due to the large oscillations in the radial position of the head of the jet, so that while the jet may not become unstable in a formal sense, it is difficult to resist characterizing the behavior as such.

The hollow conical jet neither focuses nor collimates. The large oscillations mean that it wanders considerably from the initial precession cone, but it does so without any directional preference. The external ambient medium plays almost no role in the dynamics of the jet; the cocoon is the primary influence on the exterior of the jet, just as it is for the filled and hollow cylindrical geometries. The Eichler (1983) focusing mechanism does not seem to be applicable to these flows. In the interior region, the ambient medium acts essentially as a "shock absorber." While there is a mass flow out of the interior region, the interior pressure never (on average) drops significantly. A lower interior density reduces the inertia of the gas, which makes it easier for the jet to move inward, but it is the pressure which ultimately determines how closely the jet can approach the axis. As long as the pressure forces can become sufficiently large, the jet will be pushed back toward the precession cone, preventing any permanent focusing.

V. CONSEQUENCES FOR SS 433

The implication of the preceding sections is that hollow conical jets propagate inefficiently, if at all, because of the geometric dilution and spreading of the working surface. In addition, the jets do not focus; hydrodynamic interactions maintain significant average pressure in the interior of the cone. The simulations, however, dealt with a series of parametrized variables. In this section, we ask whether or not the hydrodynamical jet can in any way be suitable as a model of the SS 433 jet system.

Suppose we attempt to match the hydrodynamic simulation into the parameters of SS 433 rather than simply as a series of dimensionless numbers. This is not meant to be a serious attempt to "model" SS 433, but only to try to connect the results to a realistic system. To this end, we state the jet luminosity and velocity to the approximate values for SS 433. The jet kinetic luminosity is taken to be $L_{40} = L_j/10^{40}$ ergs s^{-1}, based on the characteristics of the emission lines from SS 433 and on the energy required to create the "ears" of W50 (Begelman *et al.* 1980; Königl 1983). The jet velocity is $v_{\mathrm{SS}\,433} = v_j/0.26c$. If we place the outer edge of the grid at a distance of $l = 50$ pc from the source of the jet, and assume the jet propagates on the 20° half-angle precession cone before it reaches the left edge of the grid, we find that each zone has a width of ~ 0.1 pc. Recall that this is approximately twice the distance between successive windings of the jet. The left edge of the grid is ~ 5 pc from the origin, and the jet is injected at $\bar{R} = (R_{\mathrm{out}} + R_{\mathrm{in}})/2 = 1.7$ pc with width $\Delta R = (R_{\mathrm{out}} - R_{\mathrm{in}}) = 0.85$ pc. These values for the parameters imply that the jet density at the orifice is

$$\rho_j \sim 3 \times 10^{-4} m_p \ \mathrm{cm}^{-3} L_{40} v_{\mathrm{SS}\,433}^{-3} \left(\frac{\bar{R}}{2\Delta R}\right), \qquad (5.1)$$

the jet presure is

$$P_j \sim 2 \times 10^{-11} \ \mathrm{dynes\ cm}^{-2} L_{40} v_{\mathrm{SS}\,433}^{-1} \left(\frac{\bar{R}}{2\Delta R}\right)\left(\frac{M_j}{30}\right)^{-2}, \qquad (5.2)$$

and the jet temperature is

$$T_j \sim 4 \times 10^8 \ \mathrm{K}\ \mu \left(\frac{M_j}{30}\right)^{-2} v_{\mathrm{SS}\,433}^{2}, \qquad (5.3)$$

where $\rho = \mu m_p n$ relates mass and number densities. The chosen Mach number of 30 makes the jet in pressure equilibrium with an ambient pressure of 2×10^{-11} dynes. The conditions inside of W50 are not known, but we can derive a few crude order of magnitude estimates with which to work. The edge of W50 is quite sharp, presumably corresponding to a strong shock. The pressure inside W50 should then be at least several times the ambient interstellar medium (ISM) pressure; a value on the order of 10^{-11} dynes is not unreasonable. Further, this pressure gives a total internal energy of $\sim 10^{51}$ ergs, roughly consistent with the observed energetics of the W50. The ambient density and temperature are limited by the lack of observed X-ray emission in W50 (Watson *et al.* 1983). Adopting the $T_6 = T_a/10^6$ K for the temperature of the ambient medium, we obtain a density ratio of

$$\eta = \rho_j/\rho_a \sim 2.5 \times 10^{-3} T_6 \left(\frac{M_j}{30}\right)^{2} v_{\mathrm{SS}\,433}^{-2}, \qquad (5.4)$$

at the jet inlet. The isothermal sound crossing time for this set of parameters is 10^3 yr.

The choice of a Mach 30 jet means that, according to equation (3.4), the stalling radius is approximately 50 pc. However, because the density ratio is so small, the jet is well into the cocoon-dominated regime of jet propagation. Extrapolating the behavior of such a jet from the simulations we have run poses a problem of self-consistency. (Actually carrying out the specific simulation would require an enormous expenditure of computer time that would be difficult to justify for this simplistic model.) As the jet surrounds itself with spent gas, the medium through which it propagates changes. The ambient medium will play only a minor initial role in the jet evolution. If one proposes that all of W50 is a large inflated cocoon from the hollow jet, the temperature in W50 would be on order 10^{10} K, from the thermal energy associated with the large jet velocity. The cocoon density would be $\sim 10^{-5} m_p$ cm^{-3} for $P \sim 10^{-11}$ dynes (consistent with eq. [3.11] for a Mach 30 jet).

Such a gas would not produce the observed X-ray and optical emission in W50; this would have to be caused by the entrained ISM. The present hollow jet would be propagating essentially through its own spent cocoon with density ratio on order unity.

Can a purely hydrodynamical conical jet account for the "ears" of W50? In the absence of a significantly asymmetric background pressure or density distribution, a protrusion such as the ears requires the directed deposition of energy. A jet provides such direction in principle, but that directionality will be lost at large distances from a *stalled* jet. We must therefore require that the jet stall on a scale comparable to W50 and that it focus or collimate sufficiently in order to direct its momentum and energy flux primarily in the direction of the ears. If we consider only the morphological resemblance of the simulations to that of SS 433, we immediately find several differences. First, without significant focusing, the conical jets do not form any structure reminiscent of the ears of W50. Although the jet can oscillate into much smaller radii than that of the precession cone, this inevitably results in an increase of the pressure in the interior, driving the jet out away from the axis. The cocoon is preferentially inflated outside the precession cone, leaving the interior filled with shocked ambient material. These interior shocks are driven out along the axis, but they produce an extremely flat bow shock (relative to the filled jets) rather than a protrusion along the axis. The periodic compression of material inside the precession cone could serve as a natural source for the diffuse X-ray emission observed by Watson *et al.* (1983). However, in the final analysis, the failure of the conical jets to propagate, and the morphological differences between W50 and any structure observed in the simulations, suggest that a hydrodynamical model without additional physics may be inappropriate for the propagation of the SS 433 jet on the largest scales.

Is SS 433 a purely hydrodynamic jet? As discussed in § I, there is no clear answer to these questions based on the current state of the observations. Our simulations indicate, however, that the simple hydrodynamic jet we have modeled does not resemble the W50 system. If our simple hydrodynamic model is untenable, what are the alternatives? We can categorize several options.

1. The jet is focused hydrodynamically, but additional physical processes or different initial data must be used to modify the dynamics, such as radiative cooling, or heat conduction.
2. Jet focusing or collimation is achieved by other than hydrodynamic means.
3. Despite appearances, the jet is not *directly* responsible for the "ears."
4. The jet we see today has changed from the jet which generated the ears of W50.

The first category can be divided into adding new physical processes and changing the assumptions of our model. If the goal is to focus the jet, the additional physics should cool the gas inside the precession cone. The aim must be to reduce the interior pressure sufficiently rapidly to allow a pressure gradient to focus the jet as in the Eichler (1983) model. Regardless of the physical mechanism proposed to accomplish this end, care must be taken that the lost energy is accounted for. For example, the observed luminosity of the area inside the precession cone is $L \lesssim 10^{38}$ ergs s^{-1} (mostly in the IR; see Band 1987) although the observational situation is far from clear. Under ideal conditions, in which all of this energy is directly extracted from the transverse expansion of the jet, this would allow the focusing of jets with $L_j \lesssim 10^{39}$ ergs s^{-1}. This is already at the lower end of the estimates for the jet luminosities which can create the "ears" of W50. The cooling efficiency is highly unlikely to be that efficient, and a more realistic upper limit on the jet luminosity for which cooling can significantly modify the dynamics is $L_j \lesssim 10^{38}$ ergs s^{-1}. It is also unclear whether the required bias toward cooling the interior of the precession cone exists; the simulations indicate that the interior of the cone is hotter and more rarefied than the exterior, which would suggest that the interior cools less efficiently than the exterior.

Another approach is to ask what initial conditions or assumptions in the simulations can be changed without adding additional physics. It is possible that the assumption of axisymmetry, which forces the axial focusing of shocks, distorts the results significantly. If the shocks were not coherently focused at the axis, the interior pressure would not be as effective in preventing focusing. The cone would not oscillate in phase; compression of the interior on one side of the cone could be compensated for by expansion on the other side. It is not clear whether this would result in focusing or in even more chaotic motion of the jet channel. This idea could be studied in a manner analogous to the studies of slab jets by looking at the propagation of two slab jets injected at an angle to each other (see Norman and Hardee 1988). Alternatively, the interior pressure might be reduced by altering the steady jet injection to a periodic injection. If the jet has "holes" in it that allow the interior gas to leak through, the interior pressure can be reduced. Moreover, the interior gas may be able to leak through the jet without significantly perturbing the jet; this would help to damp the radial oscillations that lead to the R^2 dilution of the jet momentum flux density. Considering that the observations of the jet show that it has a "blob-like" structure on the smallest scales, this effect must be present in the real jet to some degree. This might be studied by using a "two-phase" jet model in which most of the momentum and energy is carried in pulses of dense, cool gas, and in which the interpulse part of the jet is filled with tenuous material. Finally, the jet could be taken to be a *filled* conical jet rather than a hollow conical jet. In this case the transverse expansion lowers the interior pressure leading to a refocusing of the jet.

In the second category, we mention the possibility of a magnetically dominated jet. Such a jet might be able to collimate in a manner reminiscent of the magnetically confined model for overpressured filled jets. Direct numerical situations (LPMB88; Norman, private communication) have succeeded in propagating such overpressured jets. An added difficulty for the SS 433 jet is that magnetic hoop stress must overcome the large transverse ram pressure of the jet rather than the thermal pressure forces present in the filled jet simulations. Magnetohydrodynamic simulations of hollow, conical jets are needed to explore this idea.

Models in the third category are hard to justify because of the near-perfect alignment of the jet axis and W50. However, Katz (1986) mentions such a model in which the ears are created by radiation flux from the central object, rather than from the hydrodynamic jet. The greatest radiation flux from a thick accretion disk would naturally be aligned with the jet.

A related possibility is that the jet we see today is not the jet which generated the ears. The jet's precession cone may be slowly widening; the ears would have formed when the cone was much narrower. In any case, removing a causal connection between the ears at the current epoch has the virtue of explaining why there is little evidence for energetic jet interactions with the W50 remnant (apart from the ears!). It avoids the discrepancy between the large implied jet kinetic luminosity $L_j \sim 10^{40}$ ergs s^{-1}, and the observed luminosity $\sim 10^{38}$ ergs s^{-1}.

To conclude, it is hardly surprising that the SS 433 jet is more complicated than an axisymmetric, conical, hydrodynamic jet. Our aim in this paper has been to draw attention to that fact. Because there clearly exist a large number of possible modifications to our simple model, the hydrodynamic jet paradigm cannot be considered dead; it is, however, more tightly constrained. Considering the powerful effects of the "turbulent" gas dynamics on the evolution of the jet, it is unlikely that a model of the SS 433 jet is complete or robust in its conclusions without including the full multidimensional, nonlinear effects of supersonic hydrodynamics.

The authors wish to thank Mitch Begelman for originally suggesting this problem, and Roger Blandford and Roger Romani for helpful discussions. The computations were performed on the Cray X-MP48 at the National Center for Supercomputing Applications. This research was supported at Caltech by a graduate fellowship from the AT&T Foundation, by NSF grant AST86-15325, and by NASA Astrophysical Theory Program grant NAGW-1301, and at Virginia by NASA Astrophysical Theory Program grant NAGW-764 and NSF grant PHY88-02747.

REFERENCES

Band, D. L. 1987, *Pub. A.S.P.*, **99**, 1269.
Begelman, M. C., Sarazin, C. L., Hatchett, S. P., McKee, C. F., and Arons, J. 1980, *Ap. J.*, **238**, 722.
Davidson, K., and McCray, R. 1980, *Ap. J.*, **241**, 1082.
Downes, A. J. B., Pauls, T., and Salter, C. J. 1986, *M.N.R.A.S.*, **218**, 393.
Eichler, D. 1983, *Ap. J.*, **272**, 48.
Hardee, P. E., and Norman, M. L. 1988, *Ap. J.*, **334**, 70.
Hawley, J. F., Smarr, L. L., and Wilson, J. R. 1984, *Ap. J. Suppl.*, **55**, 211.
Hjellming, R., and Johnston, K. 1982, in *IAU Symposium 97, Extragalactic Radio Sources*, ed. D. Heeschen and C. M. Wade (Dordrecht: Reidel), p. 197.
———. 1985, in *Radio Stars*, ed. R. M. Hjellming and D. M. Gibson (Dordrecht: Reidel), p. 309.
———. 1988, *Ap. J.*, **328**, 600.
Katz, J. I. 1986, *Comments Ap.*, **11**, 201.
Kirshner, R. P., and Chevalier, R. A. 1980, *Ap. J. (Letters)*, **242**, L77.
Königl, A. 1983, *M.N.R.A.S.*, **205**, 471.
Kössl, D., and Müller, E. 1988, *Astr. Ap.*, **206**, 204.
Lind, K. R., Payne, D. G., Meier, D. L., and Blandford, R. D. 1988, Caltech preprint.
Margon, B. 1984, *Ann. Rev. Astr. Ap.*, **22**, 507.
Milgrom, M., Anderson, S. F., and Margon, B. 1982, *Ap. J.*, **256**, 222.
Norman, M. L., and Hardee, P. E. 1988, *Ap. J.*, **334**, 80.
Norman, M. L., Smarr, L. L., Winkler, K.-H. A., and Smith, M. D. 1982, *Astr. Ap.*, **113**, 285.
Norman, M. L., and Winkler, K.-H. A. 1985, *Los Alamos Science*, No. 12, p. 38.
Norman, M. L., Winkler, K.-H. A., and Smarr, L. L. 1983, in *Astrophysical Jets*, ed. A. Ferrari and A. G. Pacholczyk (Dordrecht: Reidel), p. 227.
———. 1984, in *Proc. NRAO Workshop 9, Physics of Energy Transport in Extragalactic Radio Sources*, ed. A. Bridle and J. Eilek (Green Bank: NRAO), p. 150.
Vermeulen, R. C., Schilizzi, R. T., Icke, V., Fejes, I., and Spencer, R. E. 1987, *Nature*, **328**, 309.
Watson, M. G., Willingale, R., Grindlay, J. E., and Seward, F. D. 1983, *Ap. J.*, **273**, 688.
Zealey, W. J., Dopita, M. A., and Malin, D. F. 1980, *M.N.R.A.S.*, **192**, 731.

JOHN F. HAWLEY: Department of Astronomy, University of Virginia, Charlottesville, VA 22903

CHRISTOPHER S. KOCHANEK: Theoretical Astrophysics, Caltech 130-33, Pasadena, CA 91125